Response of the Sea Breeze to Urbanization in the Pearl River Delta Region

CHENG YOU

Division of Environment and Sustainability, Hong Kong University of Science and Technology, Hong Kong, China

JIMMY CHI-HUNG FUNG

Division of Environment and Sustainability, and Department of Mathematics, Hong Kong University of Science and Technology, Hong Kong, China

WAI PO TSE

Environmental Science Programs, School of Science, Hong Kong University of Science and Technology, Hong Kong, China

(Manuscript received 5 April 2018, in final form 11 March 2019)

ABSTRACT

The Pearl River delta (PRD) region has undergone rapid urbanization since the 1980s, which has had significant effects on the sea-breeze circulation in this region. Because the sea breeze plays an important role in pollutant transportation and convective initiation in the PRD region, it is meaningful to study the effects of urbanization on the sea breeze. In this study, three numerical experiments were conducted from 2 June to 31 August 2010 with land-use data from 1988, 1999, and 2010. For each simulation, characteristics of the sea breeze such as the start time, end time, intensity, height, pumping ability, and inland penetration distance were quantified. By comparing the characteristics of the sea breeze in these simulations, its response to urbanization was quantified. The results show that urbanization enhances the duration, height, and intensity of the sea breeze but blocks its inland penetration. One physical mechanism is proposed to dynamically elucidate the response of the sea breeze to urbanization. Because the urban area in the PRD region is concentrated near the coast, urbanization imposes a positive heating gradient on the coastal region and a negative heating gradient on the region farther inland. The positive heating gradient may intensify the sea breeze, and the negative heating gradient may prevent the sea breeze from propagating farther inland.

1. Introduction

The sea breeze is fueled by land–sea thermal differences in coastal regions (Simpson 1994). With the extension of urban areas in coastal cities, the thermal properties of land surface have been changed significantly, which may affect sea breezes. Much attention has been dedicated to the effects of urbanization on sea breezes. Ado (1992) found that an urban heat island near the coast can strengthen the sea breeze in the growing stage. A sea breeze from the East Sea and a lake breeze from Lake Taihu were found to intensify the heat island circulation over Shanghai (Miao and Tang 1998). A sea-breeze front can be more easily recognized with more urbanized land use, but two additional hours are needed for the sea-breeze front to penetrate farther inland (Lin et al. 2008). With the presence of an urban area, the propagation speed of the sea-breeze front may be slowed (Freitas et al. 2007; Leroyer et al. 2014). In the absence of the urban area, the head of the sea-breeze front in New York City would extend vertically to a much higher level (Thompson et al. 2007). If the urban heat island magnitude the night before is stronger, the lake-breeze fronts of Lake Michigan tend to propagate more slowly (Keeler and Kristovich 2012). Interaction among the sea breeze, the Taipei urban heat island, and the mountains was found to strengthen thunderstorms downstream of the sea breeze (Chen et al. 2007). Similar results have also been

Supplemental information related to this paper is available at the Journals Online website: https://doi.org/10.1175/JAMC-D-18-0081.s1.

Corresponding author: Cheng You, cheng.you@misu.su.se

DOI: 10.1175/JAMC-D-18-0081.1

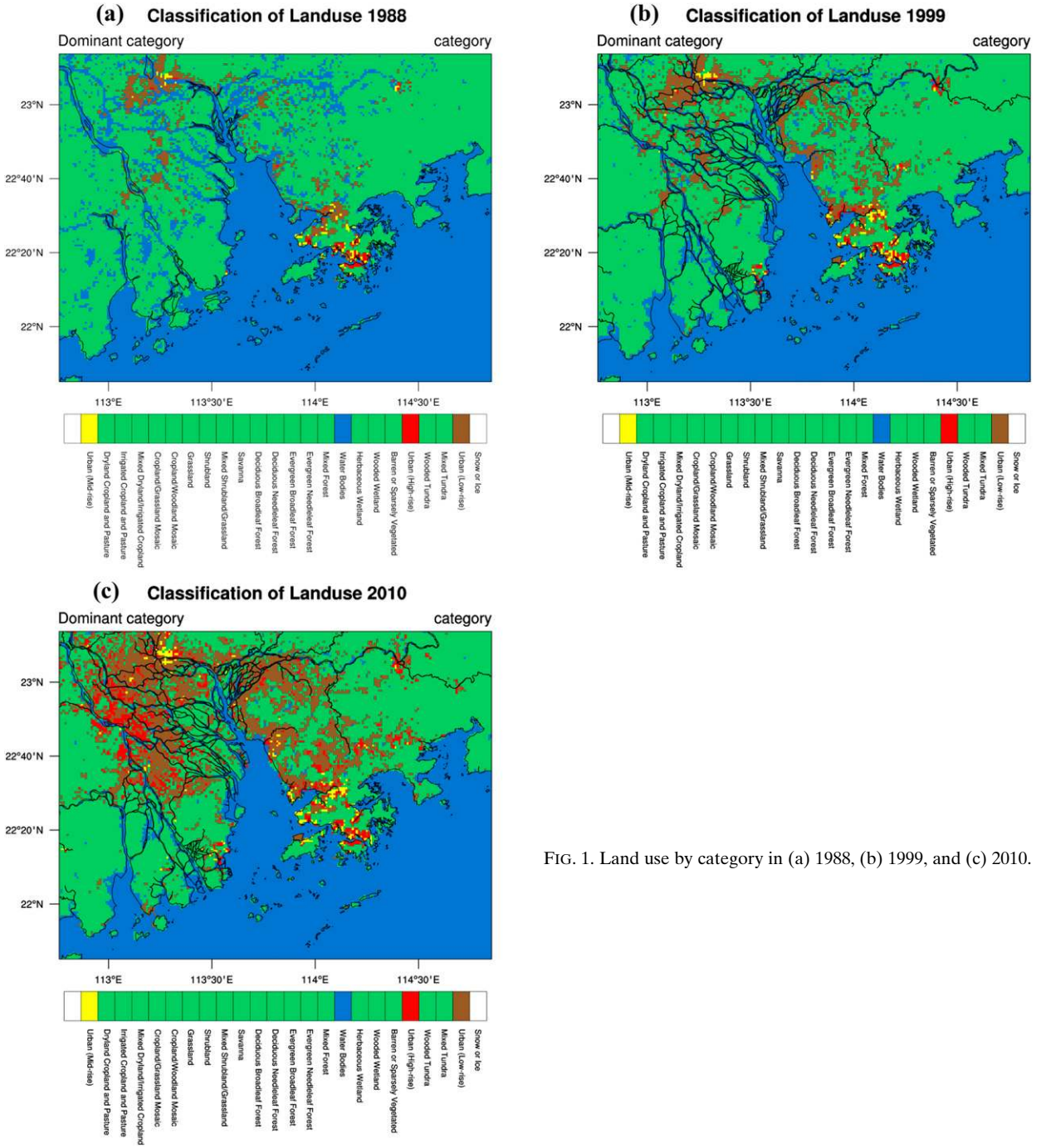

FIG. 1. Land use by category in (a) 1988, (b) 1999, and (c) 2010.

found in Houston and in central Taiwan (Shepherd et al. 2010; Lin et al. 2008).

The Pearl River delta (PRD) region has undergone rapid urbanization since the 1980s. Several researchers have focused on the effects of urbanization on sea-breeze events in this region. It was found that industrial development and urbanization in the PRD region strengthens the daytime sea-breeze circulation (Lo et al. 2007). Lu et al. (2010) found that the urbanization of Shenzhen may dramatically intensify the sea breeze to the west of Hong Kong, and similar results were also found by Wu et al. (2011). However, most of these studies focused only on case studies, which cannot illustrate the general effects of urbanization on sea breezes. In addition, these studies did not define any standard variables to quantify the onset

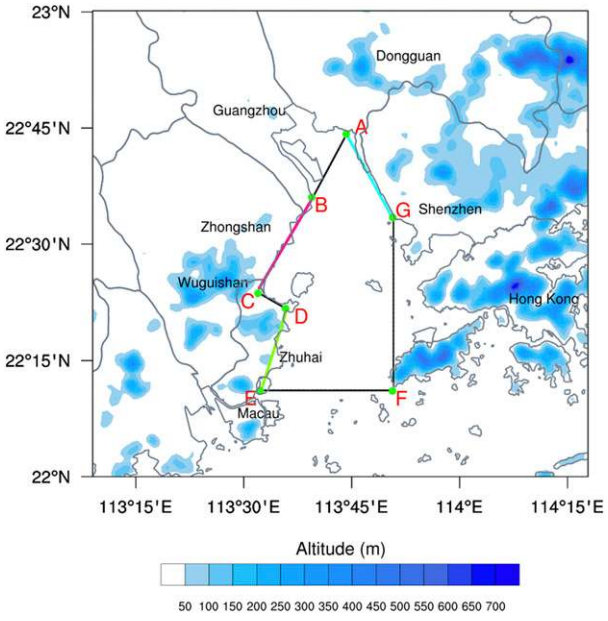

FIG. 2. Terrain and coastlines in the PRD region. The coastlines have been simplified into straight lines AG, DE, and BC.

time, cessation time, or strength of sea breezes, which makes it difficult to quantitatively compare sea-breeze events in different land-use scenarios. In this study, a method to quantitatively characterize the sea breeze is used to analyze and compare sea breezes simulated from 2 June to 31 August in 2010, with land-use data from 1988, 1999, and 2010. More information about the simulation and the method is introduced in section 2, and the statistical results are shown and discussed in section 3. In section 4, one physical mechanism is proposed to dynamically elucidate the response of the sea breeze to urbanization in the PRD region. Section 5 then concludes the paper.

2. Data and methods

As illustrated by Fig. 1, the PRD region underwent rapid urbanization between 1988 and 2010, especially in Guangzhou, Zhongshan, Dongguan, and Shenzhen (geographic places are shown in Fig. 2), and the urban area is mostly concentrated in the coastal region. To identify the effects of urbanization on sea breezes in the PRD region, three numerical experiments with the Weather Research and Forecasting (WRF) Model were conducted from 2 June to 31 August 2010 with land-use data from 1988, 1999, and 2010 (Fig. 1). In these simulations, four domains were utilized in this two-way nesting simulation and they cover eastern Asia (d01), south China (d02), the PRD region (d03), and the Pearl River estuary (d04), respectively (Fig. 3). The grid spacing for these domains are 27, 9, 3, and 1 km. The WRF terrain-following vertical coordinate contains 47 eta levels, and 17 levels are within the first kilometer. The initial and boundary condition were obtained from NCEP FNL Operational Global Analysis data with a horizontal resolution of 1° in latitude and longitude and a temporal resolution of 6 h. The Asymmetric Convective Model, version 2 (Pleim 2007a,b), was used in this simulation because it performs better

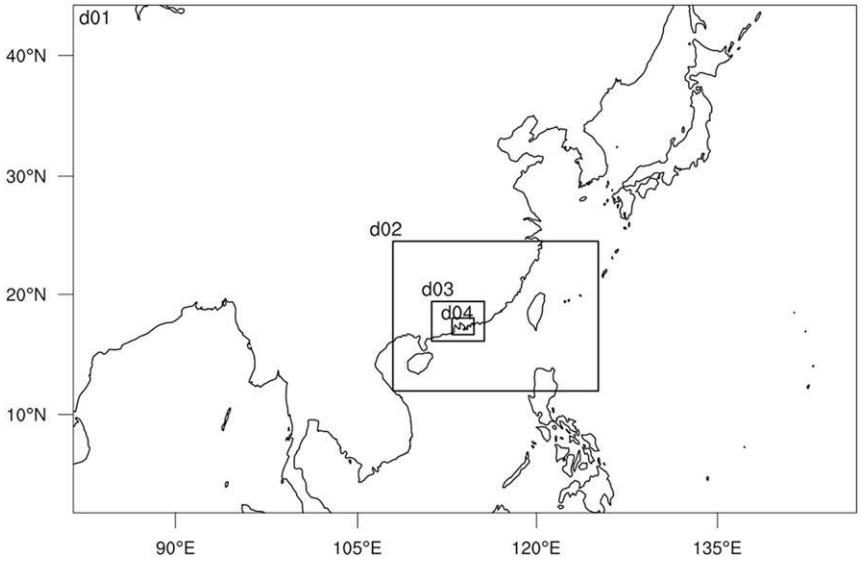

FIG. 3. Setup for the WRF domains. These four domains cover eastern Asia (d01), south China (d02), the PRD region (d03), and the Pearl River Estuary (d04). Their grid spacing are 27, 9, 3, and 1 km, respectively.

TABLE 1. The root-mean-square error of the 2-m temperature and 10-m wind speed in June, July, and August 2010. Observation data from 644 stations in the PRD region are used here for data validation.

	June	July	August
2-m temperature	1.87	2.11	1.87
10-m wind speed	1.51	1.44	1.39

than other planetary boundary layer schemes in the PRD region (Xie et al. 2012). The Rapid Radiative Transfer Model (RRTM) longwave radiation scheme (Mlawer et al. 1997), the Dudhia shortwave radiation scheme (Dudhia 1989), the WRF single-moment three-class microphysics scheme (Hong et al. 2004), and the Noah Land Surface Model (Chen and Dudhia 2001) were applied in all domains. The Grell–Devenyi ensemble cumulus scheme (Grell and Dévényi 2002) was applied in d01 and d02. The root-mean-square error of the 2-m temperature in each summer month ranged from 1.87° to 2.11°C, whereas it ranged from 1.39 to 1.51 m s^{-1} for 10-m wind speed (Table 1). The evaluation

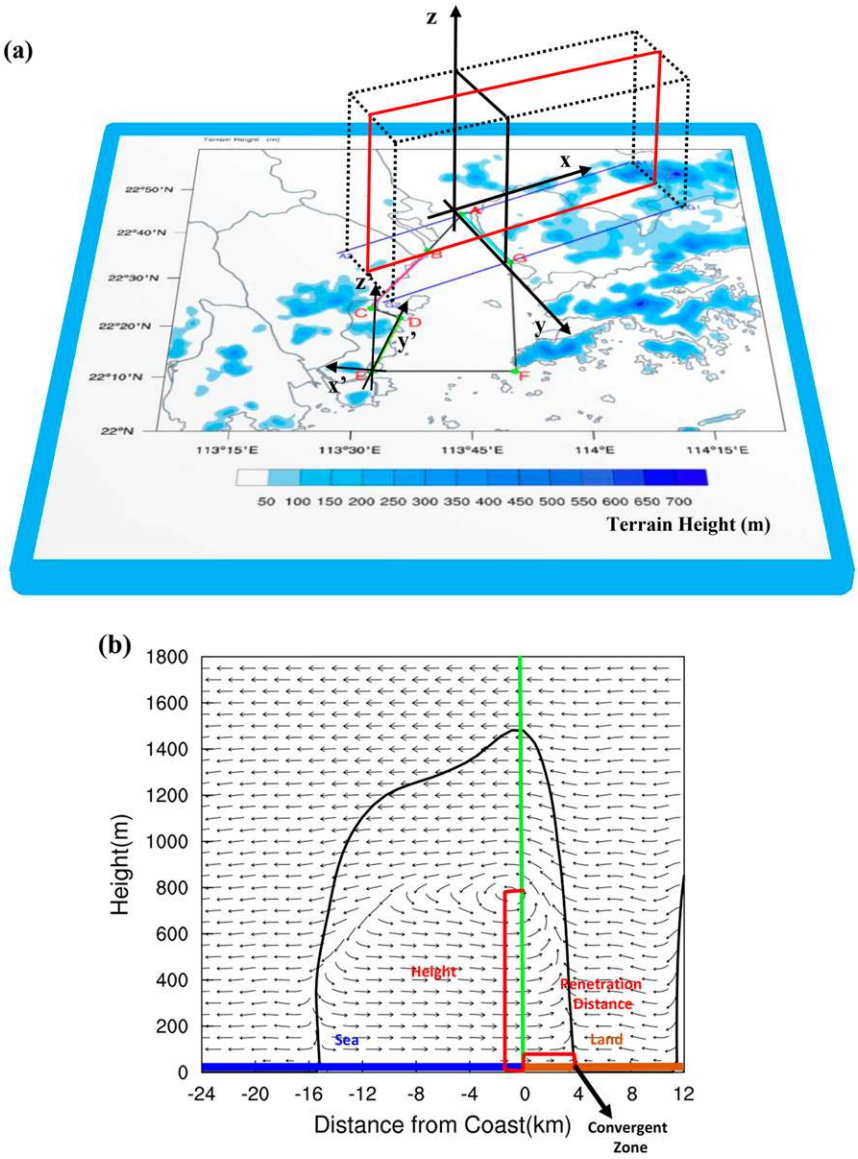

FIG. 4. (a) The Cartesian coordinate system in which diagnostic variables like frontogenesis functions are evaluated. The red rectangle is the mean vertical cross section that is achieved by averaging the three-dimensional physical variables in the black box over the *y* direction. (b) An example of average sea-breeze circulation in the mean vertical cross section along coast AG. The solid black line is the boundary of sea-breeze circulations. The coast lies on the origin point of the *x* axis. The positive *x* axis represents land, and the negative values represent the sea.

TABLE 2. The characteristics of sea-breeze events along coast AG that could be found in all numerical experiments Exp1, Exp2 and Exp3, including start time (LT), end time (LT), duration (h), intensity ($m\,s^{-1}$), maximum penetration distance D_{SB} (km), pumping ability f_H ($m^2\,s^{-1}$), and height H_{SB} (m). Relative to Exp1, the earlier start time, postponed end time, enhanced duration, intensity, D_{SB}, f_H, and H_{SB} in Exp2 are highlighted in boldface and the postponed start time, earlier end time, reduced duration, intensity, D_{SB}, f_H, and H_{SB} are in italics and similar for Exp3 but relative to Exp2. A slash indicates that the sea breeze could not be separated from the background wind and therefore it is impossible to evaluate D_{SB}, f_H, and H_{SB}.

	Exp1 (1988)						Exp2 (1999)						Exp3 (2010)					
Date	Start time	End time	Duration	Intensity	D_{SB}	f_H	H_{SB}	Start time	End time	Duration	Intensity	D_{SB}	f_H	H_{SB}	Start time	End time	Duration	Intensity	D_{SB}	f_H	H_{SB}
11 Jun 2010	1200	1700	5	2.11	/	/	/	1200	**1800**	**6**	**2.82**	/	/	/	1200	**1900**	**7**	*2.66*	/	/	/
20 Jul 2010	1000	1700	7	3.14	13	1379	550	1000	1700	7	**3.61**	**15**	*1375*	550	**0900**	1700	**8**	*3.51*	15	**1716**	**650**
23 Jul 2010	1000	2000	10	1.18	/	/	/	**0800**	**2100**	**13**	**1.43**	/	/	/	0800	*2000*	*12*	*1.34*	/	/	/
1 Aug 2010	1000	1900	9	2.39	22	1445	600	1000	1900	9	**2.5**	22	**1645**	**650**	**0900**	1900	**10**	*2.34*	*19*	**1835**	**700**
2 Aug 2010	1100	1700	6	1.41	38	1970	750	1100	**2100**	**10**	1.41	**40**	*1395*	*700*	1100	*1600*	*5*	**2.06**	*35*	*1378*	700
4 Aug 2010	1200	1400	2	0.83	/	/	/	**1100**	**1500**	**4**	*0.62*	/	/	/	1100	**1700**	**6**	**0.97**	**36**	**1937**	**900**
7 Aug 2010	1100	1600	5	2.81	11	568	350	1100	1600	5	**3.13**	*6*	**597**	*300*	*1200*	**1800**	**6**	*2.57*	*4*	**754**	**400**
24 Aug 2010	1100	1600	5	1.87	16	369	450	1100	**1700**	**6**	**2.34**	*14*	**628**	**500**	**1000**	**1800**	**8**	**2.53**	**16**	**806**	**650**
27 Aug 2010	1300	2000	7	3.05	3	575	300	**1200**	*1900*	7	**3.78**	**4**	**848**	**400**	*1300*	*1800*	*5*	*3.43*	*2*	*470*	*350*
28 Aug 2010	1400	1600	2	4.24	1	321	200	**1200**	1600	**4**	*4.07*	**4**	**549**	**300**	1200	1600	4	*3.35*	*2*	*337*	*250*
30 Aug 2010	1100	1800	7	2.55	11	1446	600	1100	**1900**	**8**	**2.58**	**15**	**1853**	**750**	1100	1900	*8*	**2.69**	*12*	**1946**	**850**
31 Aug 2010	1200	1700	5	2.08	9	521	600	1200	1700	5	**2.43**	*8*	**569**	*500*	*1300*	1700	*4*	*2.25*	*3*	**585**	500
Avg	1125	1715	5 h 50 m	2.30	13.8	955	489	**1055**	**1755**	**7**	**2.56**	**14.2**	**1051**	**517**	1055	*1750*	*6 h 55 m*	*2.47*	**14.4**	**1176**	**595**

results showed that the overall performance of WRF over the PRD region is reasonable with this configuration.

The method identified by (Cheng and Fung 2019) was used to quantitatively characterize the sea breeze in different land-use scenarios. As shown in Fig. 2, the three main coasts in the PRD region were simplified as straight lines AG, BC, and DE. We focused mainly on coasts AG and DE because coast BC has shifted considerably over the past 30 years. In this study, most variables related to coast AG were evaluated in the x, y, and z Cartesian coordinate system designed in Fig. 4a. Its y axis coincides with coast AG, and the x axis is perpendicular to coast AG. We focused mainly on variables on the mean vertical cross section (red rectangle in Fig. 4a), which is achieved by averaging the three-dimensional physical variables in the black box over the y direction. A similar method was also used for coast DE, but in the x', y', and z' coordinate system (Fig. 4a).

The horizontal wind field is decomposed into divergent and nondivergent parts with the method introduced by Cao and Xu (2011) and Xu et al. (2011). Along coasts AG (DE), the normal divergent velocity V_D and normal original velocity V_O, which both are x (x') components of divergent velocity and original velocity, were spatially averaged in direction y (y'). Positive signals of V_D were taken as sea-breeze events along each coast if they began after sunrise and finished in one day (see section 1 in the online supplemental material). The start time of a sea breeze was defined as the time at which V_D and V_O are both positive, whereas the time at which any of them will be negative was taken as the end time. V_D at a height of 50 m was taken as the intensity of the sea breeze. In the averaged vertical wind field (Fig. 4b), the height at which the V_O over the coast first changes from positive to negative was considered to be the height H_{SB} of the sea breeze. Integrated V_O over height (i.e., $f_x = \int_0^z V_O\,dz$) is also evaluated, and its zero contours (solid black line) are used to indicate the boundary of atmospheric circulation. The inland lateral boundary illustrated by f_x can also be used to estimate the maximum inland penetration distance of the sea breeze D_{SB}. In addition, f_x at height H_{SB} over the coast ($f_H = \int_0^{H_{SB}} V_O\,dz$) can also quantify the pumping ability of the sea-breeze circulation. Both f_H and H_{SB} were evaluated for separable sea-breeze events that have clear boundaries.

3. Statistical results

a. *Characteristics of the sea breeze along coast AG with different land-use scenarios*

Three numerical experiments with land-use data from 1988 (Exp1), 1999 (Exp2), and 2010 (Exp3) were

TABLE 3. Number of separable cases in Exp1, Exp2, and Exp3 along with their D_{SB}, f_H, and H_{SB}.

Numerical Expt	Exp1	Exp2	Exp3
No. of separable cases	16	16	16
Inland penetration distance (km)	14.6	15	16.7
Pumping ability ($m^3 s^{-1}$)	904	966	1277
Height (m)	466	525	628

designed to illustrate the effects of urbanization on the sea-breeze circulation. The method mentioned above was used to quantify the sea breeze in the PRD region. Twenty, 19, and 20 sea-breeze events were identified in Exp1, Exp2 and Exp3, respectively, and only 12 cases in common were found in all of these three simulations. The statistical results of these 12 cases are summarized in Table 2. In Exp1, the average start time was 1125 LT, and the average end time was 1715 LT. The mean start time of sea-breeze events in Exp2 was 30 min earlier than that of Exp1 [4 cases earlier; 8 cases no change (Table 2)], and the mean end time was 40 min later [6 cases earlier, 1 case later, and the rest no change (Table 2)]. Therefore, the mean duration of the sea-breeze events in Exp2 was 70 min longer [7 cases longer; the rest no change (Table 2)]. Relative to Exp1, the increased urban land use in Exp2 and Exp3 appears to have enhanced the intensity (9 cases stronger, 2 cases weaker, and 1 no change), D_{SB} (5 cases farther, 3 cases shorter, and 1 no change), f_x (7 cases stronger; 2 weaker), and H_{SB} (5 cases higher, 3 lower, and 1 no change) of the sea-breeze events. Although the start time, end time, duration, and D_{SB} of the sea breezes in Exp2 are comparable to those in Exp3, f_x (7 cases stronger; 3 weaker), and H_{SB} (6 cases higher, 2 weaker, and 2 no change) in Exp3 are still obviously enhanced relative to Exp2. If considering all of the separable sea-breeze cases (16 separable cases were found in all these three simulations), the height and pumping ability of the sea breeze both appeared to be enhanced with more urban land use in Exp2 and Exp3 but the inland penetration distance did not change as obviously (Table 3). However, the average lateral boundary of the sea-breeze circulation in Exp1 reached farther inland than that in Exp3 at the start time, the strongest time, and the end time (Fig. 11, described in more detail below, only illustrates the boundary at the strongest time). A similar phenomenon was also found by Freitas et al. (2007).

Urbanization can enhance sea breezes and strengthen their pumping ability. At the start time, the vertical profiles of V_O and f_x in Exp3 almost overlap with those in Exp2, and both are larger than those in Exp1 (Fig. 5a). In addition, the sea breeze and sea-breeze circulation in Exp2 and Exp3 are lifted into higher levels. Similarly, at strongest time, V_O and f_H in Exp2 and Exp3 are larger than that in Exp1 (Figs. 5c,d). For Exp2, urbanization

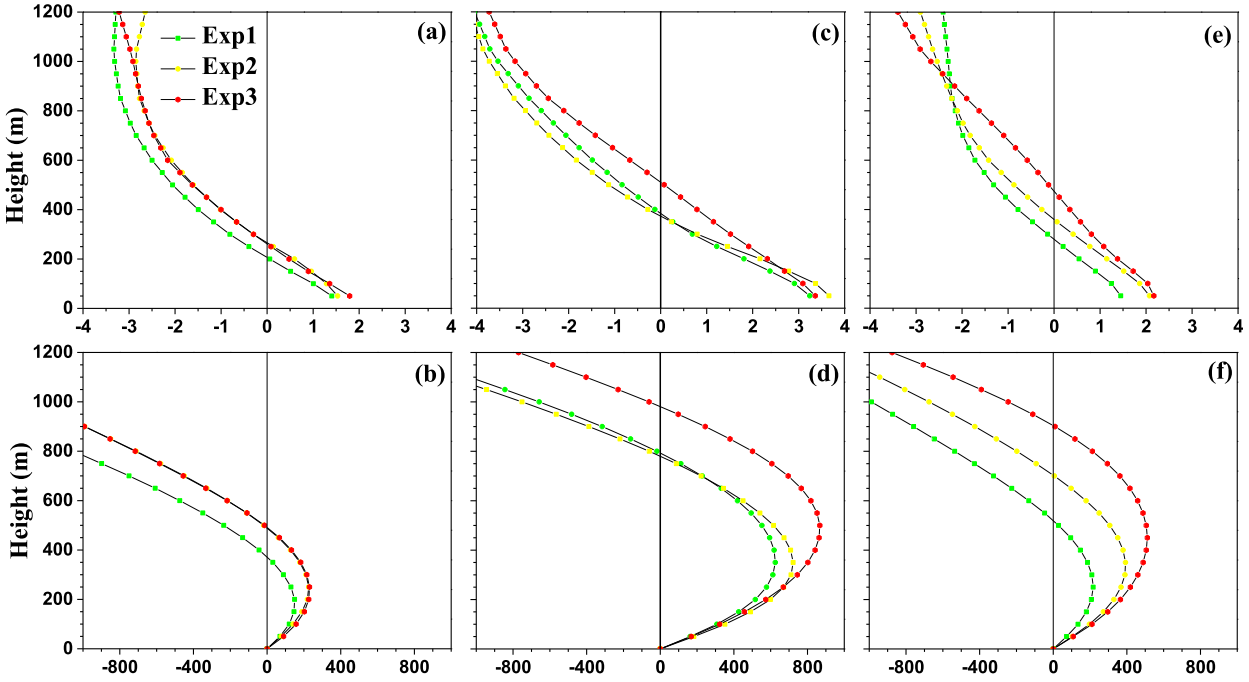

FIG. 5. Average vertical profiles of (top) V_O ($m s^{-1}$) and (bottom) f_x ($m^3 s^{-1}$) in Exp1, Exp2, and Exp3 over coast AG at the (a) (b) start time, (c) (d) strongest time, and (e) (f) end time. The maximum value of f_x is f_H.

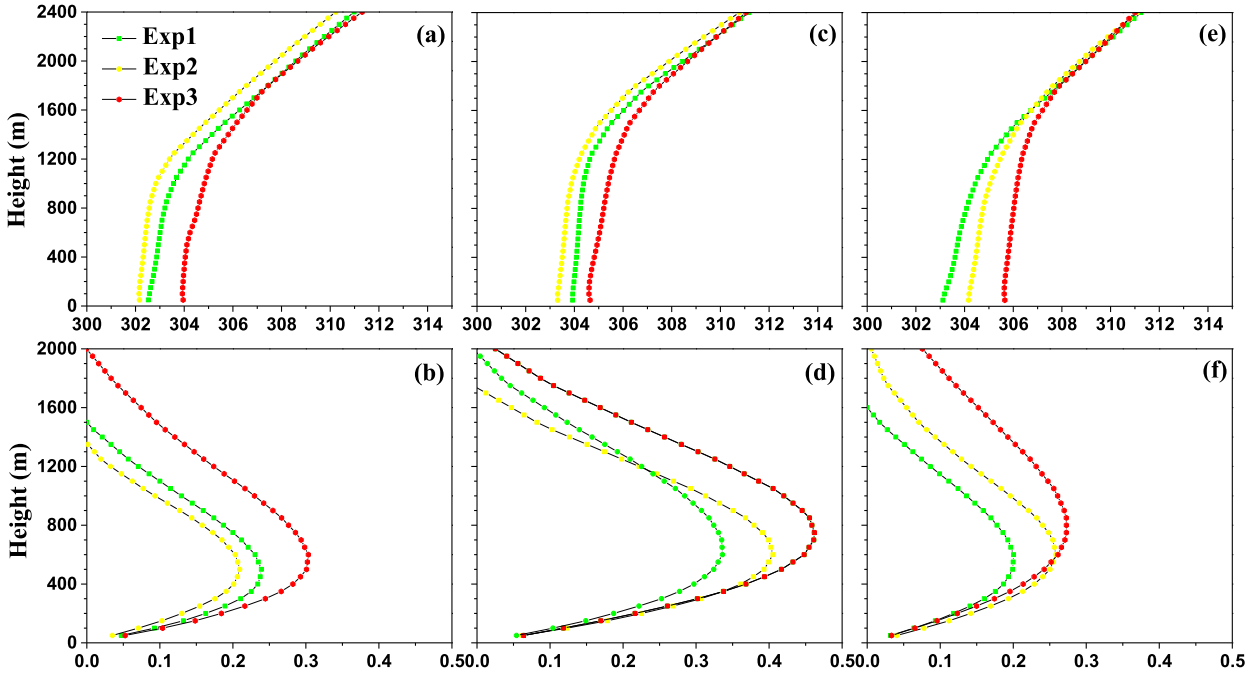

FIG. 6. As in Fig. 5, but for (top) vertical velocity (m s^{-1}) and (bottom) potential temperature (K) (a) over the convergent zone near coast AG.

apparently intensifies the near-surface sea breeze, but the height of the sea breeze and sea-breeze circulation remain the same as in Exp1 (Fig. 5c). In Exp3, however, the sea breeze and sea-breeze circulation are more than 100 m higher. The near-surface sea breeze in Exp2 is slightly stronger than that in Exp3, whereas at a higher level, it is much smaller than that in Exp3. At the end time, with more urban land use, the sea breeze is more intensive from the ground to the top, in conjunction with its pumping ability (Figs. 5e,f). Meanwhile, the sea breeze and sea-breeze circulation are also higher.

The vertical motion above the convergent zone can also be intensified by urbanization (Figs. 6b,d,f), and the vertical profile of the potential temperature becomes better mixed or even more unstable with more urban land use (Figs. 6a,c,e). In addition, the height of the lifted inversion layer is also increased. At the start time, the vertical motion in Exp2 is not obviously increased (Fig. 6b), and its profile of potential temperature is almost parallel with that in Exp1 (Fig. 6a). In Exp3, however, the vertical motion is intensified dramatically. With stronger vertical motion, the near-surface layer in Exp3 becomes better mixed, and the height of the inversion layer is increased. At the strongest time, with a more urbanized PRD, the vertical motion intensifies in the convergent zone near coast AG (Fig. 6d). Meanwhile, the vertical profile of potential temperature in Exp2 is still parallel with that in Exp3 (Fig. 6c), whereas the near-surface potential temperature in Exp3 decreases slightly with height, and the inversion layer is lifted higher (Fig. 6c). Similarly, at the end time, the vertical motion increases and the atmospheric boundary layer becomes less stable as a result of urbanization in both Exp2 and Exp3 (Fig. 6e). For Exp3, a thin unstable layer can be found near the surface. In addition, at this moment, the lifted inversion layer in Exp3 is also higher than those in the other two numerical experiments.

b. Characteristics of the sea breeze along coast DE with different land-use scenarios

Along coast DE, 29, 33, and 35 sea-breeze events were identified respectively in Exp1, Exp2, and Exp3, and 23 cases in common were found in all of these three simulations. Similar to coast AG, the intensity, height, and duration of sea-breeze events at coast DE are also enhanced by urbanization (Table 4). Their end time is also generally postponed by nearly 30 min, whereas with more urban land use in Exp2 and 3 the start time of the sea breeze is 13 min later than that in Exp1. Therefore, the duration is slightly increased, but not as dramatically as for coast AG. The general intensity of sea breezes at 50 m is modulated by urbanization in a different manner from that for coast AG. The intensities in Exp2 and Exp3 change only slightly along coast DE, whereas they change significantly along

TABLE 4. Same as table 2 but for sea breezes along coast DE.

Date	Exp1 (1988)							Exp2 (1999)							Exp3 (2010)						
	Start time	End time	Duration	Intensity	D_{SB}	f_H	H_{SB}	Start time	End time	Duration	Intensity	D_{SB}	f_H	H_{SB}	Start time	End time	Duration	Intensity	D_{SB}	f_H	H_{SB}
11 Jun 2010	0900	1500	6	1.88	35	551	450	0900	1500	6	**2.13**	*32*	643	450	0900	1500	6	**2.15**	**35**	**672**	**500**
28 Jun 2010	0800	1700	9	1.06	34	839	450	**0700**	**1900**	**12**	**1.20**	**56**	829	450	0700	*1800*	*11*	**1.26**	56	*685*	**450**
29 Jun 2010	0700	2100	14	0.98	/	/	/	*0800*	*1900*	*11*	**1.61**	**5**	**560**	**350**	0800	1900	11	**1.80**	**33**	**1417**	**600**
30 Jun 2010	0900	1700	8	2.39	7	875	450	0900	1800	9	2.39	*6*	*843*	*400*	**0800**	1800	**10**	**2.42**	6	**875**	**450**
2 Jul 2010	1300	1500	2	3.61	/	/	/	1300	1500	2	*3.16*	/	/	/	1300	1500	2	**3.26**	/	/	/
10 Jul 2010	0900	1800	9	1.92	4	294	300	*1300*	1800	*5*	**2.01**	**5**	**658**	**400**	**1000**	1800	**8**	**2.17**	**6**	**940**	**500**
11 Jul 2010	1300	1700	4	2.76	5	218	250	*1400*	1700	*3*	*2.69*	*3*	**293**	250	1400	1700	3	*2.65*	**4**	*220*	250
12 Jul 2010	1100	1800	7	2.06	6	567	400	**1000**	1800	**8**	**2.17**	6	**670**	400	1000	**1900**	**9**	*2.11*	**7**	*561*	400
15 Jul 2010	1200	1700	5	0.77	/	/	/	*1300*	1700	*4*	**0.98**	/	/	/	1300	*1600*	*3*	**1.08**	/	/	/
18 Jul 2010	1000	1800	8	1.22	35	1078	550	**0900**	1800	**9**	**1.58**	*11*	**1254**	550	0900	1800	9	**2.07**	*9*	**1458**	**600**
24 Jul 2010	1000	1800	8	1.56	6	810	500	1000	1800	8	*1.50*	**16**	**1133**	**600**	1000	1800	8	**1.55**	*5*	*590*	*450*
31 Jul 2010	1500	1700	2	1.75	5	159	300	1500	**1800**	**3**	*1.39*	/	/	/	1500	1800	3	**1.40**	**5**	**197**	**250**
3 Aug 2010	1000	1500	5	2.45	21	557	500	*1100*	**1600**	5	*2.34*	*19*	*458*	500	1100	1600	5	**2.43**	*10*	**500**	*450*
4 Aug 2010	1000	1800	8	3.25	29	712	450	1000	1800	8	**3.48**	*16*	**721**	450	1000	1800	8	**3.61**	16	**758**	450
10 Aug 2010	0900	1800	9	0.85	/	/	/	0900	**1900**	**10**	**0.98**	/	/	/	0900	*1800*	*9*	**1.19**	/	/	/
11 Aug 2010	0900	1700	8	2.07	8	1103	600	0900	**1800**	**9**	*1.85*	8	*1079*	600	*1000*	**1900**	9	**2.19**	8	**1630**	**800**
12 Aug 2010	1100	1700	6	1.86	4	621	450	1100	**1800**	**7**	**2.02**	**5**	**764**	**500**	1100	1800	7	**2.32**	*4*	**862**	500
14 Aug 2010	0900	1700	8	2.62	9	1125	600	0900	1700	8	**2.72**	*6*	*922*	*500*	*1000*	1700	*7*	**3.02**	6	**925**	**550**
16 Aug 2010	1100	1800	7	1.88	7	528	450	1100	*1700*	*6*	**2.20**	*3*	*334*	*350*	1100	**1800**	**7**	**2.25**	**33**	**715**	**550**
17 Aug 2010	1000	1300	3	1.24	/	/	/	1000	**1400**	**4**	*0.90*	/	/	/	1000	1400	4	**1.17**	/	/	/
18 Aug 2010	0900	1600	7	1.46	16	151	250	*1000*	**2000**	**10**	*1.34*	**18**	**411**	**450**	1000	**2100**	**11**	**1.48**	*16*	*371*	450
30 Aug 2010	1100	1600	5	3.11	13	193	250	**1000**	1600	**6**	*2.82*	*12*	**277**	**300**	*1200*	1600	*4*	**3.35**	**13**	**364**	**400**
Avg	1014	1657	6 h 44 m	1.94	13.6	577	400	*1027*	**1725**	**6 h 57 m**	**1.98**	*13.4*	**697**	**441**	1027	**1727**	**7**	**2.13**	**15.1**	**763**	**478**

coast AG. Nevertheless, with more urban land use, the sea breeze along coast DE pumps more air from the sea to the land and extends vertically to a higher level. If considering all separable sea-breeze events, the inland penetration distances in Exp2 and Exp3 are shortened by urbanization (Table 5). This effect is also supported by Fig. 12 (described in more detail below) which illustrates that the lateral boundary of the sea breeze in Exp1 is always located farther inland than that in Exp3. The effects of urbanization on the vertical profile of the sea breeze at coast DE are similar to those at coast AG. The difference is that the height of the inversion layer near coast DE is almost the same in each scenario.

4. Physical mechanism to modulate the urbanization effects on sea-breeze circulation

To illustrate the effects of urbanization on the sea breeze at coasts DE and AG, the potential temperature, pressure, solenoid term, atmospheric friction term, and vorticity acceleration were evaluated on the mean vertical cross section (Fig. 4a) and averaged among all sea-breeze events at the start time, strongest time, and end time. The potential temperature gradient, solenoid term, and atmospheric friction term over the coast are greater at all moments in Exp3 than in Exp1; however, the pressure field changes little (Figs. 11 and 12, below). The sea breeze in Exp3 is higher than that in Exp1 at the start time and the strongest time, but the inland penetration distance in Exp3 is reduced, especially for the sea breeze along coast DE (Figs. 11 and 12, below). In Exp1 at coast DE, as they propagate gradually inland, the sea-breeze circulation and the mountain-valley circulation (see section 2 in the online supplemental material) on the land develop into a new circulation on a larger horizontal scale (green line in Fig. 12a, below). At the end time, all three circulations (one sea-breeze circulation and two mountain-valley circulations) have combined into one. However, in Exp3, the average sea-breeze circulation (black line in Fig. 12 a, below) does not merge with any other circulations, which shortens its inland penetration distance.

The physical mechanism of sea-breeze circulation proposed by Cheng and Fung (2019) is used in this section to explain this phenomenon. As concluded by Cheng and Fung (2019), for the sea breeze in the PRD region, the positive vorticity acceleration that stimulates sea-breeze circulation is mainly contributed by the solenoid term, which in turn is mostly controlled by the temperature gradient because the pressure gradient force is nearly constant during the development of the sea-breeze circulation.

TABLE 5. As in Table 3, but for sea breezes at coast DE.

Numerical Expt	Exp1	Exp2	Exp3
No. of separable cases	21	23	24
Inland penetration distance (km)	14.0	11.0	12.7
Pumping ability ($m^3 s^{-1}$)	574	622	691
Height (m)	412	433	460

Considering the importance of the temperature gradient, the frontogenesis function was thus used to diagnose the magnitude and spatial distribution of the four factors [Eqs. (2)–(5)] that contribute to the temperature gradient. According to the frontogenesis function (Ninomiya 1984),

$$\frac{d}{dt}|\nabla_p \ln T_v| = \frac{d}{dt}|\nabla_p \ln\theta_v| = \mathrm{FG1} + \mathrm{FG2} + \mathrm{FG3} + \mathrm{FG4}, \tag{1}$$

where the four forcing terms on the right-hand side are

$$\mathrm{FG1} = \frac{1}{|\nabla_p \ln\theta_v|}\left[\nabla_p \ln\theta_v \cdot \nabla_p\left(\frac{d}{dt}\ln\theta_v\right)\right], \tag{2}$$

$$\mathrm{FG2} = -\frac{1}{2|\nabla_p \ln\theta_v|}\left[\left(\frac{\partial}{\partial x}\ln\theta_v\right)^2 + \left(\frac{\partial}{\partial y}\ln\theta_v\right)^2\right] \times\left(\frac{\partial u}{\partial x} + \frac{\partial v}{\partial y}\right), \tag{3}$$

$$\mathrm{FG3} = -\frac{1}{|\nabla_p \ln\theta_v|}\left\{\frac{1}{2}\left[\left(\frac{\partial}{\partial x}\ln\theta_v\right)^2 - \left(\frac{\partial}{\partial y}\ln\theta_v\right)^2\right] \times\left(\frac{\partial u}{\partial x} - \frac{\partial v}{\partial y}\right) + \frac{\partial \ln\theta_v}{\partial x}\frac{\partial \ln\theta_v}{\partial y}\left(\frac{\partial v}{\partial x} + \frac{\partial u}{\partial y}\right)\right\}, \quad \text{and} \tag{4}$$

$$\mathrm{FG4} = -\frac{1}{|\nabla_p \ln\theta_v|}\left[\frac{\partial \ln\theta_v}{\partial p}(\nabla_p \ln\theta_v \cdot \nabla_p \omega)\right]. \tag{5}$$

In the above equations, θ_v is virtual potential temperature, ∇_p is horizontal gradient operator on an isobaric surface, u and v are horizontal wind components, and ω is vertical wind component. FG1 and FG4 evaluate the effects of heterogeneous diabatic and adiabatic heating, respectively, on the temperature gradient, and FG2 and FG3 quantify the effects of convergence and deformation, respectively, on the temperature gradient. As discussed by Cheng and Fung (2019), among these four factors FG1 (diabatic heating) is the ultimate driving force of the sea-breeze circulation, and it can be offset by FG4 (adiabatic heating). At the same time, the sea breeze can also be sustained by convergence and deformation in the convergent zone.

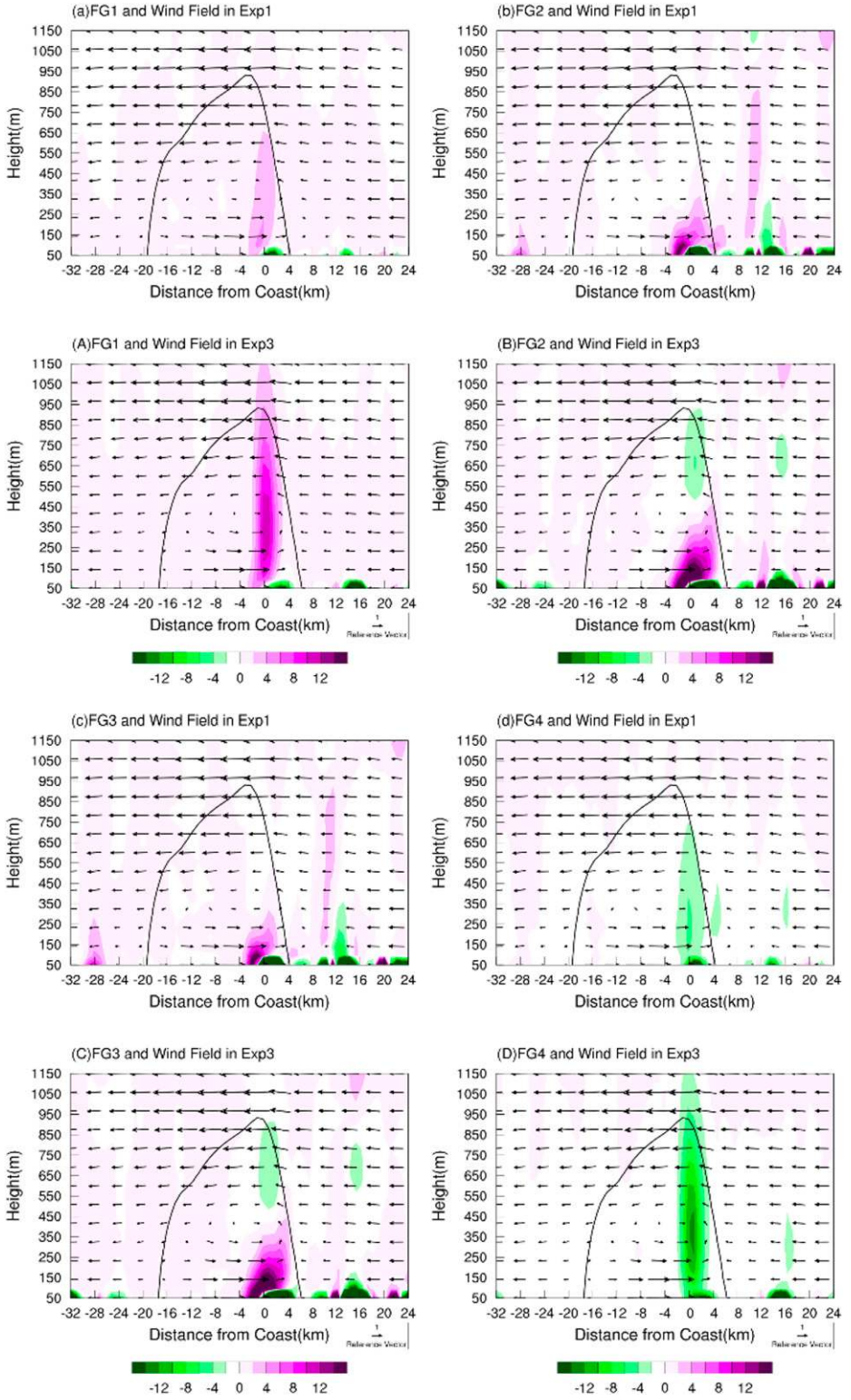

FIG. 7. Average (a) FG1 (10^{-11} K m^{-1} s^{-1}), (b) FG2 (10^{-12} K m^{-1} s^{-1}), (c) FG3 (10^{-12} K m^{-1} s^{-1}), and (d) FG4 (10^{-11} K m^{-1} s^{-1}) along coast AG in Exp1. The thick black line is the zero contour of f_x, which can approximate the boundary of the sea-breeze circulation. (A)–(D) As in (a)–(d), but for Exp3.

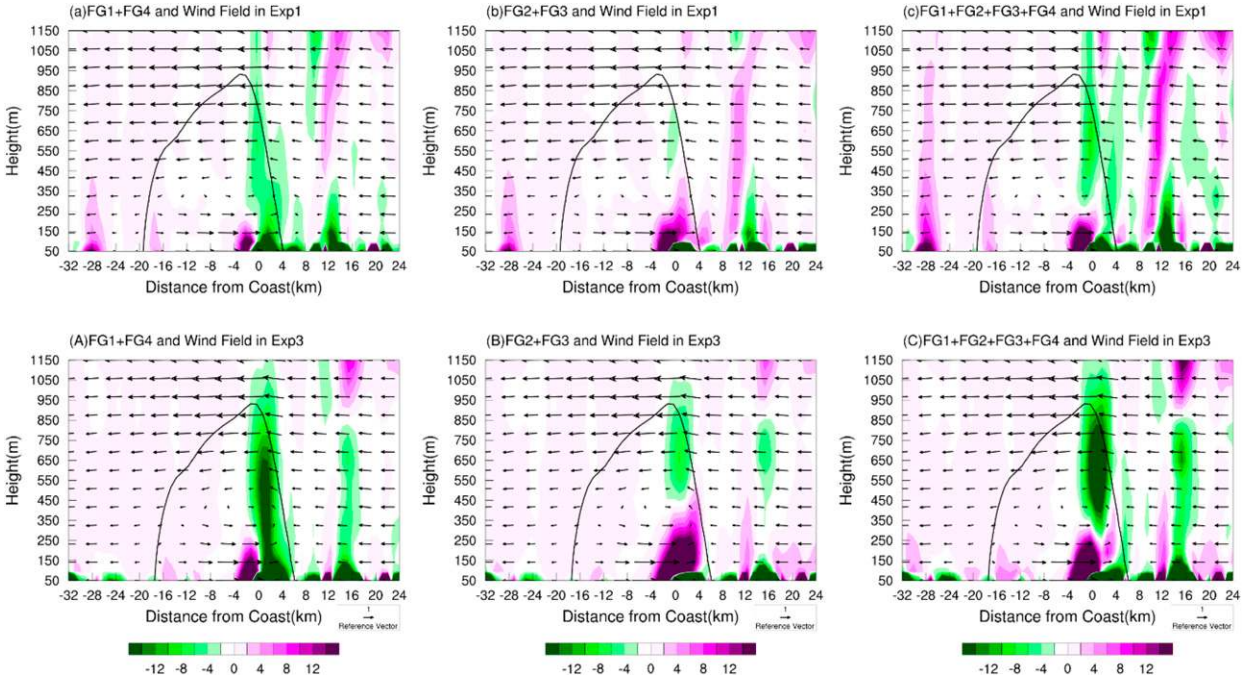

FIG. 8. Average (a),(A) FG1 + FG4 (10^{-11} K m^{-1} s^{-1}), (b),(B) FG2 + FG3 (10^{-12} K m^{-1} s^{-1}), and (c),(C) FG1 + FG2 + FG3 + FG4 (10^{-11} K m^{-1} s^{-1}) along coast AG in (top) Exp1 and (bottom) Exp3. The thick black line is the boundary of the sea-breeze circulation.

Frontogenesis functions were evaluated in the mean vertical cross section along coast AG (Fig. 4a). As shown in Fig. 7, urbanization has significant effects on frontogenesis functions. With more urban land use in Exp3, the diabatic heating and adiabatic cooling on the land is increased (Figs. 7A,D). Hence, the positive effects of FG1 on the temperature gradient are offset by the negative effects from FG4, and their overall effects

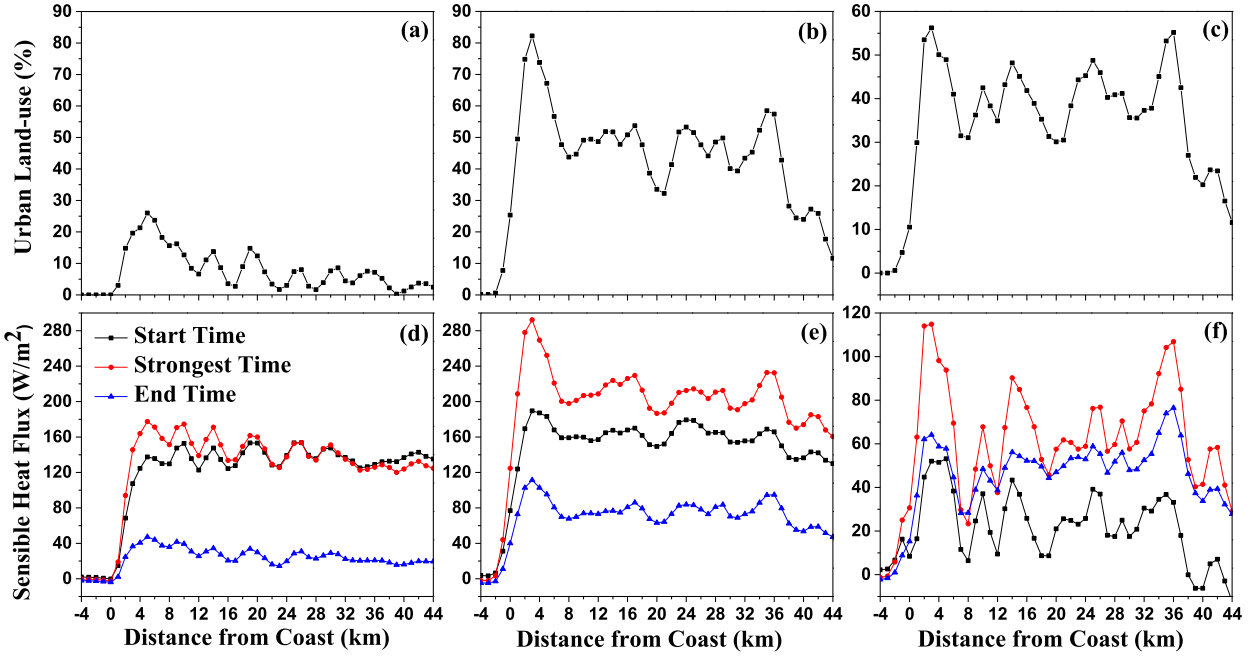

FIG. 9. Average relative area of urban land use near coast AG in (a) Exp1 and (b) Exp3, along with (c) the difference between (a) and (b). Also shown is average surface sensible heat flux (W m^{-2}) near coast AG at the start time (black line), strongest time (red line), and end time (blue line) in (d) Exp1 and (e) Exp3, along with (f) the difference between (d) and (e). The coast lies at the origin point of the x axis. The positive x axis indicates land, and the negative values represent the sea.

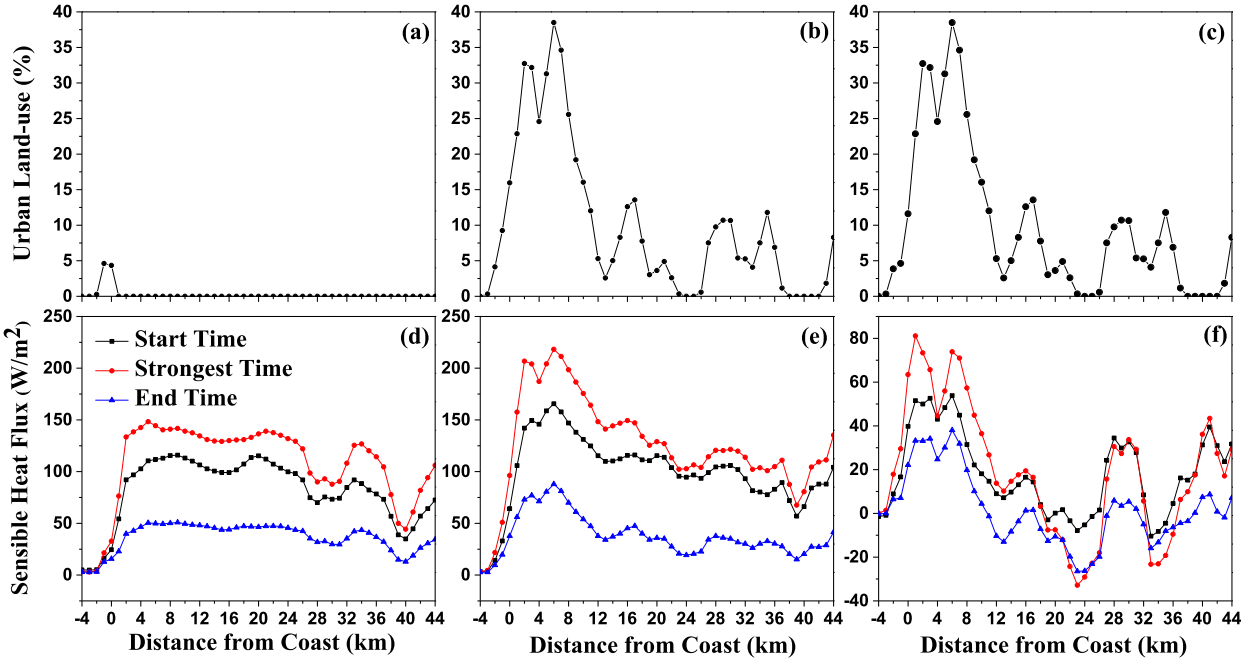

FIG. 10. Similar to Fig. 9, but for coast DE.

(FG1 + FG4) are still enhanced by urbanization (Fig. 8C). The convergence and deformation effects (FG2 and FG3) from the offshore region to the convergent zone are apparently intensified (Figs. 7B,C), which may contribute to enhancement of the temperature gradient and sea-breeze circulation there. Meanwhile, FG2 and FG3 among the inverse flow over the coastal region are decreased dramatically by urbanization. Similar results also can be found along coast DE.

Corresponding to the enhanced FG1 near coasts AG and DE in Exp3, the surface sensible heat flux is also increased there with greater urban land use (Figs. 9 and 10). Because the urban region is concentrated in the coastal region along these two coasts (Figs. 9b and 10b), the surface sensible heat flux increases inland first and reaches its maximum at the most urbanized region (Figs. 9e and 10e). It then shows an obvious decrease farther inland. Therefore, a positive heating gradient is imposed from the coast to the most urbanized region, and the temperature gradient is thus increased (Figs. 11a and 12a). However, a negative heating gradient is imposed on the region farther inland; this negative gradient is conducive to the

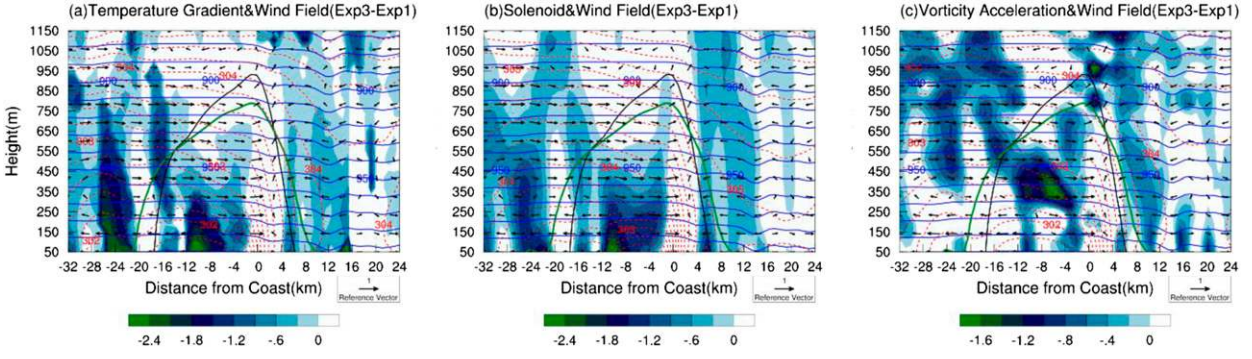

FIG. 11. The (a) temperature gradient difference (color shading; 10^{-6} K m^{-1}), (b) solenoid difference (color shading; 10^{-7} s^{-2}), and (c) vorticity acceleration difference (color shading; 10^{-7} s^{-2}), along with the wind field difference [vectors; identical in (a)–(c)] between Exp1 and Exp3 at the strongest time near coast AG. The blue and red lines respectively show average pressure and potential temperature contours [in Exp1 for (a) and (c); in Exp3 for (b)]. The thick green and black lines show the average boundary of the sea-breeze circulation in Exp1 and Exp3, respectively.

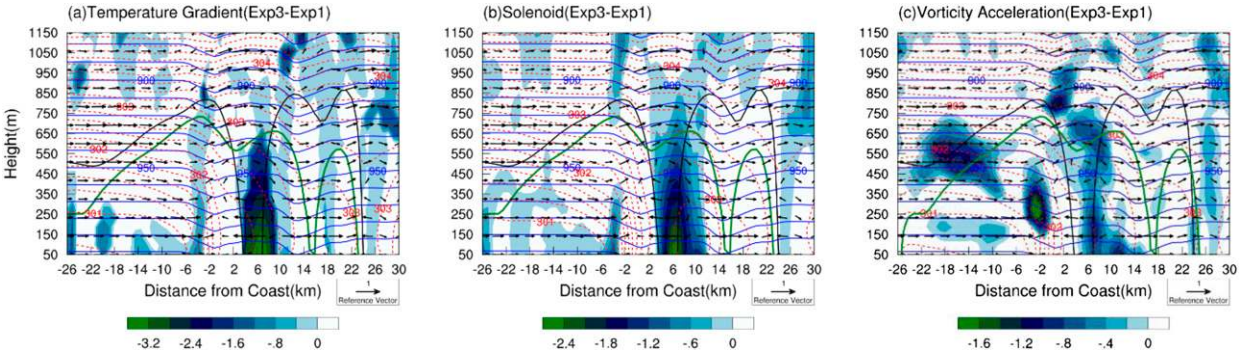

FIG. 12. Similar to Fig. 11, but for coast DE.

negative temperature gradient difference between Exp1 and Exp3 (Figs. 11a and 12a), which could induce a negative solenoid difference between Exp1 and Exp3 (Figs. 11b and 12b). This negative solenoid difference could intensify the development of anomalous negative vorticity acceleration that could stimulate a negative vortex in front of the sea-breeze circulation and suppress its inland propagation (Figs. 11c and 12c). In contrast, the positive heating gradient over the coast increases the temperature gradient and hence intensifies the solenoid term there (Figs. 11b and 12b). The enhanced solenoid term could offset the increased negative effects of atmospheric friction and contribute positively to vorticity acceleration (Figs. 11c and 12c). Consequently, the sea-breeze circulation is intensified in Exp3.

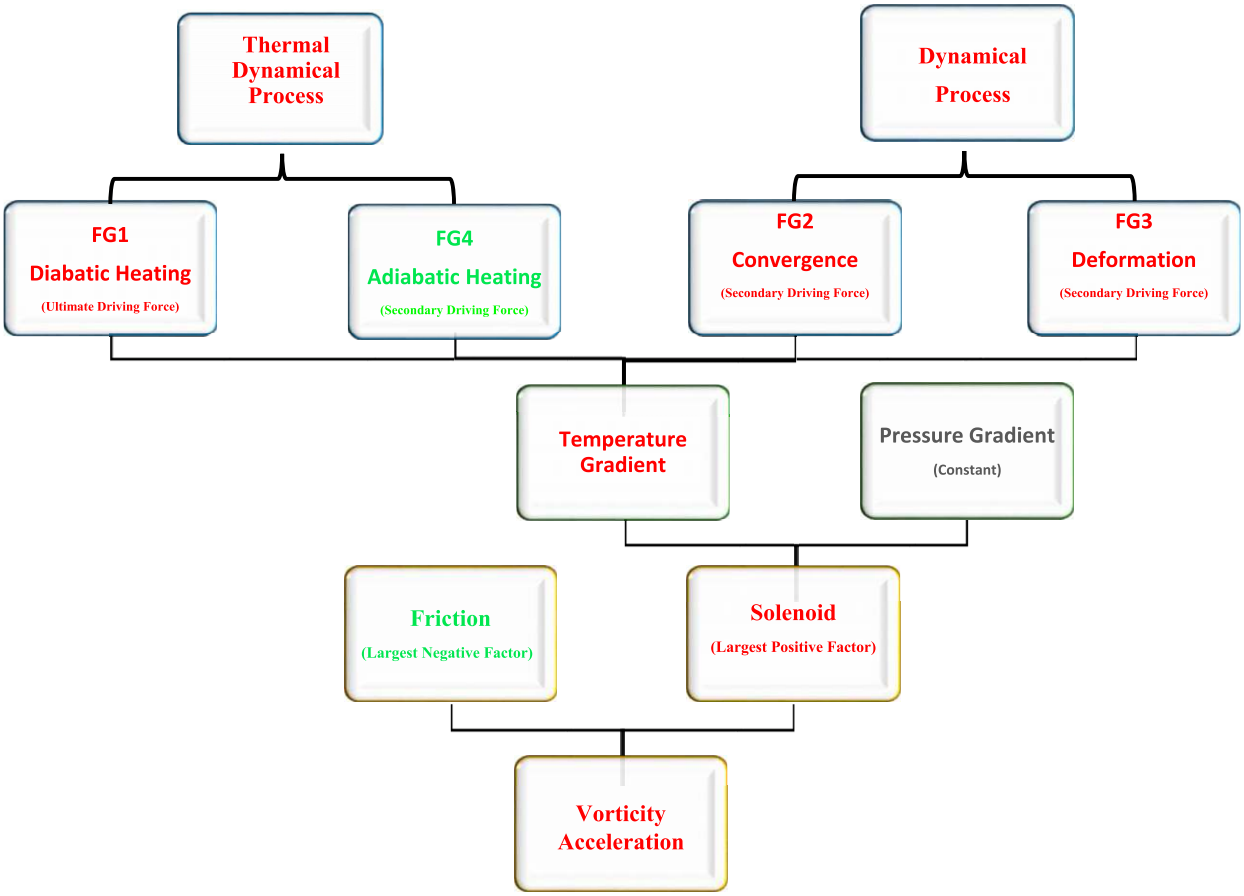

FIG. 13. Flowchart of the relationship between the variables used to diagnose the dynamic process of sea-breeze circulation in this study.

5. Conclusions

In this study, three numerical experiments using land-use data from 1988, 1999, and 2010 were conducted to quantitatively characterize the response of the sea-breeze circulation to the rapid urbanization of the PRD region. The results show that with more urban land use the duration, height, pumping ability, and intensity of the sea breeze are obviously enhanced, whereas its inland penetration distanced is shortened. In the convergent zone, vertical motion is intensified and the boundary layer becomes better mixed. In addition, the near-surface unstable layer is more obvious and the inversion layer is lifted to a higher level. Because urban land use in the PRD region is concentrated in coastal regions, from the coastal region to the most urbanized area, a positive heating gradient anomaly is imposed by urbanization, whereas a negative heating gradient anomaly can be found from the most urbanized area to somewhere farther inland. This positive heating gradient anomaly in the coastal region contributes to the enhancement of FG1 and the temperature gradient. The increased temperature gradient strengthens the solenoid term and thus intensifies the vorticity acceleration, which could fuel sea-breeze circulation. The relationships among these variables are shown in Fig. 13. However, a negative heating anomaly is conducive to a negative vorticity acceleration anomaly, which could prevent the sea-breeze circulation (positive vortex) from propagating farther inland by stimulating one negative vortex immediately in front of the sea-breeze circulation.

Acknowledgments. We thank Dr. Jie Cao (CAS Institution of Atmospheric Physics) and Prof. Qin Xu (NOAA/National Severe Storms Laboratory) for providing the source code of wind decomposition. We appreciate the assistance of the Hong Kong Observation, which provided the meteorological data. This work was supported by NSFC/RGC Grant N_HKUST631/05, NSFC-FD Grant U1033001, and RGC Grants 16303416 and 16300715.

REFERENCES

Ado, H. Y., 1992: Numerical study of the daytime urban effect and its interaction with the sea breeze. *J. Appl. Meteor.*, **31**, 1146–1164, https://doi.org/10.1175/1520-0450(1992)031<1146:NSOTDU>2.0.CO;2.

Cao, J., and Q. Xu, 2011: Computing streamfunction and velocity potential in a limited domain of arbitrary shape. Part II: Numerical methods and test experiments. *Adv. Atmos. Sci.*, **28**, 1445–1458, https://doi.org/10.1007/s00376-011-0186-5.

Chen, F., and J. Dudhia, 2001: Coupling an advanced land surface–hydrology model with the Penn State–NCAR MM5 Modeling System. Part I: Model implementation and sensitivity. *Mon. Wea. Rev.*, **129**, 569–585, https://doi.org/10.1175/1520-0493(2001)129<0569:CAALSH>2.0.CO;2.

Chen, T.-C., S.-Y. Wang, and M.-C. Yen, 2007: Enhancement of afternoon thunderstorm activity by urbanization in a valley: Taipei. *J. Appl. Meteor. Climatol.*, **46**, 1324–1340, https://doi.org/10.1175/JAM2526.1.

Cheng, Y., and J. C. H. Fung, 2019: Characteristics of sea-breeze circulation in the Pearl River delta region and its dynamical diagnosis. *J. Appl. Meteor. Climatol.*, **58**, 741–755, https://doi.org/10.1175/JAMC-D-18-0153.1.

Dudhia, J., 1989: Numerical study of convection observed during the Winter Monsoon Experiment using a mesoscale two-dimensional model. *J. Atmos. Sci.*, **46**, 3077–3107, https://doi.org/10.1175/1520-0469(1989)046<3077:NSOCOD>2.0.CO;2.

Freitas, E. D., C. M. Rozoff, W. R. Cotton, and P. L. S. Dias, 2007: Interactions of an urban heat island and sea-breeze circulations during winter over the metropolitan area of São Paulo, Brazil. *Bound.-Layer Meteor.*, **122**, 43–65, https://doi.org/10.1007/s10546-006-9091-3.

Grell, G. A., and D. Dévényi, 2002: A generalized approach to parameterizing convection combining ensemble and data assimilation techniques. *Geophys. Res. Lett.*, **29**, 1693, https://doi.org/10.1029/2002GL015311.

Hong, S.-Y., J. Dudhia, and S.-H. Chen, 2004: A revised approach to ice microphysical processes for the bulk parameterization of clouds and precipitation. *Mon. Wea. Rev.*, **132**, 103–120, https://doi.org/10.1175/1520-0493(2004)132<0103:ARATIM>2.0.CO;2.

Keeler, J. M., and D. A. R. Kristovich, 2012: Observations of urban heat island influence on lake-breeze frontal movement. *J. Appl. Meteor. Climatol.*, **51**, 702–710, https://doi.org/10.1175/JAMC-D-11-0166.1.

Leroyer, S., S. Belair, S. Z. Husain, and J. Mailhot, 2014: Subkilometer numerical weather prediction in an urban coastal area: A case study over the Vancouver metropolitan area. *J. Appl. Meteor. Climatol.*, **53**, 1433–1453, https://doi.org/10.1175/JAMC-D-13-0202.1.

Lin, C.-Y., F. Chen, J. C. Huang, W.-C. Chen, Y.-A. Liou, W.-N. Chen, and S.-C. Liu, 2008: Urban heat island effect and its impact on boundary layer development and land–sea circulation over northern Taiwan. *Atmos. Environ.*, **42**, 5635–5649, https://doi.org/10.1016/j.atmosenv.2008.03.015.

Lo, J. C. F., A. K. H. Lau, F. Chen, J. C. H. Fung, and K. K. M. Leung, 2007: Urban modification in a mesoscale model and the effects on the local circulation in the Pearl River delta region. *J. Appl. Meteor. Climatol.*, **46**, 457–476, https://doi.org/10.1175/JAM2477.1.

Lu, X., K. C. Chow, T. Yao, A. K. H. Lau, and J. C. H. Fung, 2010: Effects of urbanization on the land sea breeze circulation over the Pearl River Delta region in winter. *Int. J. Climatol.*, **30**, 1089–1104, https://doi.org/10.1002/joc.1947.

Mlawer, E. J., J. Taubman, P. D. Brown, M. J. Iacono, and S. A. Clough, 1997: Radiative transfer for inhomogeneous atmospheres: RRTM, a validated correlated-*k* model for the longwave. *J. Geophys. Res.*, **102**, 16 663–16 682, https://doi.org/10.1029/97JD00237.

Ninomiya, K., 1984: Characteristics of baiu front as a predominant subtropical front in the summer Northern Hemisphere. J. Meteor. Soc. Japan. *Ser. II*, 62, 880–894, https://doi.org/10.2151/jmsj1965.62.6_880.

Pleim, J. E., 2007a: A combined local and nonlocal closure model for the atmospheric boundary layer. Part I: Model description

and testing. *J. Appl. Meteor. Climatol.*, **46**, 1383–1395, https://doi.org/10.1175/JAM2539.1.

——, 2007b: A combined local and nonlocal closure model for the atmospheric boundary layer. Part II: Application and evaluation in a mesoscale meteorological model. *J. Appl. Meteor. Climatol.*, **46**, 1396–1409, https://doi.org/10.1175/JAM2534.1.

Shepherd, J. M., M. Carter, M. Manyin, D. Messen, and S. Burian, 2010: The impact of urbanization on current and future coastal precipitation: A case study for Houston. *Environ. Plann.*, **37B**, 284–304, https://doi.org/10.1068/b34102t.

Simpson, J. E., 1994: *Sea Breeze and Local Winds.* Cambridge University Press, 234 pp.

Thompson, W. T., T. Holt, and J. Pullen, 2007: Investigation of a sea breeze front in an urban environment. *Quart. J. Roy. Meteor. Soc.*, **133**, 579–594, https://doi.org/10.1002/qj.52.

Wu, J.-B., K.-C. Chow, J. C. H. Fung, A. K. H. Lau, and T. Yao, 2011: Urban heat island effects of the Pearl River Delta city clusters—Their interactions and seasonal variation. *Theor. Appl. Climatol.*, **103**, 489–499, https://doi.org/10.1007/s00704-010-0323-6.

Xie, B., J. C. H. Fung, A. Chan, and A. Lau, 2012: Evaluation of nonlocal and local planetary boundary layer schemes in the WRF model. *J. Geophys. Res.*, **117**, D12103, https://doi.org/10.1029/2011JD017080.

Xu, Q., J. Cao, and S. Gao, 2011: Computing streamfunction and velocity potential in a limited domain of arbitrary shape. Part I: Theory and integral formulae. *Adv. Atmos. Sci.*, **28**, 1433–1444, https://doi.org/10.1007/s00376-011-0185-6.

Miao, M.-Q., and Tang, Y.-H., 1998: Interaction between sea and land breeze and heat island circulation during the summer over the delta region of the Yangtze River and urbanization effect on climate. *Plateau Meteor.*, **17**, 280–289.